ADVANCES IN ATMOSPHERIC SCIENCES, VOL. 33, JANUARY 2016, 10–20

Ensemble Transform Sensitivity Method for Adaptive Observations

Yu ZHANG[1,2,3], Yuanfu XIE[3*], Hongli WANG[3,4], Dehui CHEN[5], and Zoltan TOTH[3]

[1]*Nanjing University of Information Science and Technology, Nanjing* 210044
[2]*Chinese Academy of Meteorological Science, Beijing* 100081
[3]*Global Systems Division, Earth System Research Laboratory, NOAA, Boulder, CO* 80305, *USA*
[4]*Cooperative Institute for Research in the Atmosphere, Colorado State University, Fort Collins, CO* 80523, *USA*
[5]*National Meteorological Centre, Beijing* 100081

(Received 23 January 2015; revised 11 May 2015; accepted 15 June 2015)

ABSTRACT

The Ensemble Transform (ET) method has been shown to be useful in providing guidance for adaptive observation deployment. It predicts forecast error variance reduction for each possible deployment using its corresponding transformation matrix in an ensemble subspace. In this paper, a new ET-based sensitivity (ETS) method, which calculates the gradient of forecast error variance reduction in terms of analysis error variance reduction, is proposed to specify regions for possible adaptive observations. ETS is a first order approximation of the ET; it requires just one calculation of a transformation matrix, increasing computational efficiency (60%–80% reduction in computational cost). An explicit mathematical formulation of the ETS gradient is derived and described. Both the ET and ETS methods are applied to the Hurricane Irene (2011) case and a heavy rainfall case for comparison. The numerical results imply that the sensitive areas estimated by the ETS and ET are similar. However, ETS is much more efficient, particularly when the resolution is higher and the number of ensemble members is larger.

Key words: adaptive observation, high impact weather, ensemble transform

Citation: Zhang, Y., Y. F. Xie, H. L. Wang, D. H. Chen, and Z. Toth, 2016: Ensemble transform sensitivity method for adaptive observations. *Adv. Atmos. Sci.*, **33**(1), 10–20, doi: 10.1007/s00376-015-5031-9.

1. Introduction

For high-impact weather (HIW) events, adaptive mobile observation instruments or vehicles can be deployed to improve analysis quality and forecast accuracy. Several field campaigns have shown that observations sampled in dynamically sensitive areas have positive impacts on numerical weather prediction (Majumdar et al., 2001; Majumdar et al., 2011). For example, 1–2 day forecast skill was increased by assimilating targeted data deployed in the Fronts and Atlantic Storm Track Experiment and the North Pacific Experiments (Joly et al., 1997; Joly et al., 1999; Langland et al., 1999a; Langland et al., 1999b). Assimilation of adaptive observations significantly reduced typhoon track forecast errors over the western North Pacific and the Atlantic (Aberson, 2003; Wu et al., 2007a; Aberson et al., 2011; Chou et al., 2011).

A major challenge is to identify sensitive areas for deploying the adaptive observations in the hours or days ahead of HIW events. There are several approaches that have been developed to estimate sensitive areas, such as the singular vector method (Palmer et al., 1998; Buizza and Montani, 1999), the conditional nonlinear optimal perturbation method (Mu et al., 2009; Wang et al., 2011), and the adjoint sensitivity method (Wu et al., 2007b, 2009). In general, an adjoint model is usually required in the above three approaches. In addition, ensemble-based methods, such as the ensemble transformation (ET) method (Bishop and Toth, 1999), the ensemble transform Kalman filter (ETKF) method (Bishop et al., 2001), and ensemble sensitivity (Ancell and Hakim, 2007) are widely used in field campaigns (Chang et al., 2013; Xie et al., 2013).

The ensemble-based methods are less demanding computationally and have been extensively employed in practical applications (Ancell and Hakim, 2007; Ito and Wu, 2013). These methods consider sensitivity in the subspace spanned by the ensemble forecasts and are computationally inexpensive in operational centers where ensemble forecasts are routinely produced. Among these methods, ET (Bishop and Toth, 1999; hereafter BT1999) provides a practical method for adaptive observations. It has been used for targeted dropsonde deployments in winter storm reconnaissance (WSR) (Szunyogh et al., 2000). Later, ETKF was used to identify the sensitive region in WSR (Szunyogh et al., 2002). The dropsonde data collected over these sensitive areas improved the weather forecasts over the continental United States and

* Corresponding author: Yuanfu XIE
E-mail: yuanfu.xie@noaa.gov

Alaska (Szunyogh et al., 2000). However, the impact of dropsonde data may be limited in global forecasts (Hamill et al., 2001), and high-resolution observation datasets are suggested for HIW (Bauer et al., 2011, Berger et al., 2011).

It is noted that ET is still expensive for high-resolution applications or those applications with large numbers of ensemble members. ET has been used at relatively coarse resolutions and a few vertical levels, e.g., usually three vertical levels at the National Centers for Environmental Prediction (NCEP), and a relatively small number of ensemble members (30–60). As resolutions increase for HIW applications, the computational cost grows exponentially. This is because ET, as well as the ETKF, has been implemented to exhaust all possible observation deployments. For example, it currently estimates sensitive areas by adding an observation at every analysis grid location, horizontally and vertically, and calculating the ensemble transformation and the reduction of forecast variance for each observation. Because of the use of a matrix decomposition of ensemble covariance, the computational cost also increases as a cubic function of the number of ensemble members. For high-resolution adaptive observation applications, or those with large numbers of ensemble members, the computational cost could be significant. ETKF can also be computationally expensive, the same as the ET method (Bishop et al., 2001). In order to further improve these methods for fine scale HIW applications, efficiency is an important factor to investigate.

A new ET-based sensitivity (ETS) method is proposed in this paper to specify sensitive regions for adaptive observations. The proposed method calculates the sensitivity (gradient) of forecast error variance reduction in terms of analysis error variance reduction. The newly proposed ETS method is the first order approximation of the original perturbation ET method and reduces computational cost because only a single transformation matrix calculation is required.

This paper is organized as follows. In section 2, we review the ET method. In section 3, we describe how ETS calculates the sensitivity with a single transformation matrix calculation. We compare sensitive regions using ET and ETS for a hurricane case and a heavy rainfall case in section 4. Conclusions and discussions are presented in section 5.

2. Review of the ET method

First, we review the ET method (BT1999), with some matrix notations used to simplify the discussion (see Table 1). This review in matrix forms helps illustrate the ETS derivation.

2.1. *Forecast error estimation using a transformation matrix*

Let $\boldsymbol{E}(t)$ denote a set of ensemble forecasts at a given forecast time t. This $\boldsymbol{E}(t)$ is a matrix with M rows and K columns, where M is the number of gridded values of all the state variables and K is the number of ensemble members. Then, the ensemble perturbation matrix $\boldsymbol{X}_{\rm e}$ is also an $M \times K$ matrix,

$$\boldsymbol{X}_{\rm e}(t) = \boldsymbol{E}(t) - \overline{\boldsymbol{E}}\,, \tag{1}$$

where $\overline{\boldsymbol{E}}$ is the ensemble mean and also an $M \times K$ matrix, but all columns are the same ensemble mean vector.

Here is the adaptive observation strategy in ET: Use a set of ensemble forecasts $\boldsymbol{E}(t)$ to determine which possible deployments of observational resources at a future analysis time $t_{\rm fa}$ will minimize the expected prediction error of forecasts for the verification time $t_{\rm v}$, which are initialized with, inter alia, the supplemental data taken at $t_{\rm fa}$ (BT1999).

Let $\boldsymbol{X}_{\rm e}(t_{\rm fa})$ denote the perturbations at $t_{\rm fa}$, $\boldsymbol{X}_{\rm e}(t_{\rm v})$ the perturbations at the $t_{\rm v}$, and $\boldsymbol{Y}(t_{\rm fa})$ the ensemble perturbations after assimilating a set of data from a possible adaptive obser-

Table 1. Important symbols.

Symbols		Descriptions
$t_{\rm fa}$	Symbol/subscript	Targeting time.
$t_{\rm v}$	Symbol/subscript	Verification time.
K	Scalar	Number of ensemble members.
M	Scalar	Number of elements in the state vector.
$\boldsymbol{I}$	Scalar	Number of possible deployments of the adaptive observation scheme
$\boldsymbol{E}(t)$	Matrix: $M \times K$	A set of ensemble forecasts at a given forecast time t.
$\overline{\boldsymbol{E}}$	Matrix: $M \times K$	The ensemble mean—all columns are the same ensemble mean vector.
$\boldsymbol{X}_{\rm e}(t)$	Matrix: $M \times K$	The ensemble perturbations—the K columns are the ensemble perturbations about the ensemble mean forecasts.
$\boldsymbol{C}$	Matrix: $K \times K$	The transformation matrix.
$\boldsymbol{Y}(t_{\rm fa})$	Matrix: $M \times K$	The ensemble perturbations after assimilating a set of data from a possible observation deployment. $Y(a) = X_{\rm e}(a)C$
$\boldsymbol{A}_{\rm e}(t_{\rm fa})$	Matrix: $M \times M$	The ensemble-based error covariance at targeting time.
$\boldsymbol{P}_{\rm e}(t_{\rm v})$	Matrix: $M \times M$	The ensemble-based forecast error covariance at verification time.
$\boldsymbol{A}_{\rm g}(t_{\rm fa})$	Matrix: $M \times M$	The guessed analysis error covariance after assimilating a set of adaptive observations—the i-th diagonal element of $\boldsymbol{A}_{\rm g}$ is $\alpha_i (i = 1, \ldots, M)$.
$\boldsymbol{S}_i$	Matrix: $M \times M$	The reduction of forecast error due to the i-th adaptive deployment
$\boldsymbol{\beta}$	Scalar	The reduction rate of analysis error variance due to assimilation of the targeting observation at location l. $(l = 1, \ldots, M)$
$\wp$	Marix: $M \times M$	The projection vector over the verification areas.

vation deployment. ET finds a transformation of the ensemble perturbation $\boldsymbol{X}_{\rm e}(t_{\rm fa})$ to $\boldsymbol{Y}(t_{\rm fa})$. Such a transformation can be uniquely determined if the number of ensemble forecasts is very large and unconstrained (Anderson, 1997). Assume such a transformation exists, and denote it as a matrix $\boldsymbol{C}$, such that

$$\boldsymbol{Y}(t_{\rm fa}) = \boldsymbol{X}_{\rm e}(t_{\rm fa})\boldsymbol{C}\,. \tag{2}$$

This $\boldsymbol{C}$ is a $K \times K$ matrix.

Mathematically, the ensemble-based error covariance at the $t_{\rm a}$ approximates the truth analysis error covariance of $\boldsymbol{A}_{\rm e}(t_{\rm fa})$,

$$\boldsymbol{A}_{\rm e}(t_{\rm fa}) \approx \frac{1}{K}\boldsymbol{X}_{\rm e}(t_{\rm fa})\boldsymbol{C}\boldsymbol{C}^{\rm T}\boldsymbol{X}_{\rm e}(t_{\rm fa})^{\rm T}\,. \tag{3}$$

The ensemble-based forecast error covariance at $t_{\rm v}$, $\boldsymbol{P}_{\rm e}(t_{\rm v})$, can be approximated by

$$\boldsymbol{P}_{\rm e}(t_{\rm v}) = \frac{1}{K}\boldsymbol{X}_{\rm e}(v)\boldsymbol{C}\boldsymbol{C}^{\rm T}\boldsymbol{X}_{\rm e}(t_{\rm v})^{\rm T}\,. \tag{4}$$

In reality, the true analysis error covariance of $\boldsymbol{A}_{\rm e}(t_{\rm fa})$ is unknown, but an approximation or guess can be estimated by a given data assimilation system (BT1999). Let $\boldsymbol{A}_{\rm g}(t_{\rm fa})$ denote the approximation of $\boldsymbol{A}_{\rm e}(t_{\rm fa})$ and Eq. (3) is approximately satisfied. Thus, forcing transformed ensemble-based error covariance to be equal to the guessed adaptive analysis error covariance,

$$\boldsymbol{A}_{\rm g}(t_{\rm fa}) = \frac{1}{K}\boldsymbol{X}_{\rm e}(t_{\rm fa})\boldsymbol{C}\boldsymbol{C}^{\rm T}\boldsymbol{X}_{\rm e}(t_{\rm fa})^{\rm T}. \tag{5}$$

The ET method finds a solution of $\boldsymbol{C}\boldsymbol{C}^{\rm T}$ satisfying Eq. (5). Note that there is really no need to explicitly calculate the transformation matrix $\boldsymbol{C}$ in the ET method but $\boldsymbol{C}\boldsymbol{C}^{\rm T}$, a product of the transformation. For the sake of simplicity, here we assume that $\boldsymbol{A}_{\rm g}$ is a full rank matrix (BT1999) and Eq. (5) can be rewritten as

$$\boldsymbol{A}_{\rm g}^{-1}(t_{\rm fa}) = K^{-1}\boldsymbol{A}_{\rm g}^{-1}(t_{\rm fa})\boldsymbol{X}_{\rm e}(t_{\rm fa})\boldsymbol{C}\boldsymbol{C}^{\rm T}\boldsymbol{X}_{\rm e}(t_{\rm fa})^{\rm T}\boldsymbol{A}_{\rm g}^{-1}(t_{\rm fa})\,. \tag{5$'$}$$

Then if $\boldsymbol{X}_{\rm e}(t_{\rm fa})$ is a full rank (e.g., a set of independent ensemble members), the matrix $\boldsymbol{X}_{\rm e}(t_{\rm fa})^{\rm T}\boldsymbol{A}_{\rm g}^{-1}\boldsymbol{X}_{\rm e}(t_{\rm fa})$ is invertible. By multiplying $\boldsymbol{X}_{\rm e}(t_{\rm fa})^{\rm T}$ and $\boldsymbol{X}_{\rm e}(t_{\rm fa})$ from the left and right of Eq. (5$'$), the solution of the product of the ET transformation matrix (BT1999) is,

$$\boldsymbol{C}\boldsymbol{C}^{\rm T} = K(\boldsymbol{X}_{\rm e}(t_{\rm fa})^{\rm T}\boldsymbol{A}_{\rm g}^{-1}\boldsymbol{X}_{\rm e}(t_{\rm fa}))^{-1}\,. \tag{6}$$

Equation (6) is an equivalent variation of the Equation (8) in BT1999. This matrix derivation of the product simplifies the derivation of BT1999.

2.2. *Measurement of adaptive observation sensitivity*

Let $\boldsymbol{\beta}$ be a parameter measuring the percentage reductions in the analysis error after a set of adaptive observations are assimilated. For example, $\boldsymbol{\beta} = 1$ means zero percent reduction, $\boldsymbol{\beta} = 0.5$ means 50% reduction etc. Let $\boldsymbol{A}_{\rm g}(\boldsymbol{\beta})$ denote the best guess of the analysis error covariance with all possible adaptive observation reduction by $\boldsymbol{\beta}$, and $\alpha_i (i = 1, \ldots, M)$ denote the i-th diagonal element of $\boldsymbol{A}_{\rm g}$.

$$\boldsymbol{A}_{\rm g}(\boldsymbol{\beta}) = {\rm diag}(\alpha_1\beta_1, \ldots, \alpha_M\beta_M). \tag{7}$$

Note that $\boldsymbol{\beta} = (\beta_1, \beta_2, \ldots)$ is a vector of all possible adaptive observation locations. Notice that we used analysis error variance only as BT1999 did. The components of $\boldsymbol{\beta}$ may or may not be equal to 1 corresponding to the given adaptive observation datasets. A value of 1 indicates no error variance reduction at this location, while a value of <1 indicates an observation at this location is assimilated. The corresponding transformation matrix $\boldsymbol{C}(\boldsymbol{\beta})$ can be calculated by (6). One can use (4) to estimate the forecast error covariance $\boldsymbol{P}_{\rm e}(t_{\rm v})$ associated with the adaptive observation scheme.

In order to calculate the observation sensitivity for an adaptive observation scheme, one has to define an output scalar measuring the sensitivity. A measurement is usually defined by an energy norm using forecast variance information from (4). For example, a total dry energy norm (Ehrendorfer et al., 1999) is expressed as,

$$\frac{1}{2}\frac{1}{D}\int_D\int_0^1 \left[u'^2 + v'^2 + \frac{c_p}{T_{\rm r}}T'^2 + RT_{\rm r}\left(\frac{{\rm pre_s}'}{{\rm pre_r}}\right)^2\right]{\rm d}\delta{\rm d}D\,, \tag{8}$$

where $(u', v', T', {\rm pre}'_{\rm s})$ are the forecast error variance of Eq. (4) corresponding to two wind components, temperature, and surface pressure. c_p, and R are specific heat at constant pressure and the gas constant of dry air, respectively (with numerical values of 1005.7 J kg^{-1} K, and 287.04 J kg^{-1} K). The integration extends over the full horizontal domain D and vertical directions δ. The $T_{\rm r}$ and ${\rm pre_r}$ are the reference temperature and pressure. In this study, zonal and meridional horizontal wind, and temperature are used to estimate the reduction of forecast error variance, since the contribution from the pressure term is very small, and thus ignored. The reference temperature is 270 K, the same as in Martin et al. (1999). In an adaptive observation measurement, it is common to use this norm to sum of the diagonal elements of $\boldsymbol{P}_{\rm e}(t_{\rm v})$ corresponding to u, v and T. Using Eqs. (4) and (8), the sum can be calculated as follows.

- A projection matrix $\wp = {\rm diag}(P_i), i = 1 \ldots M$, where $P_i = 1$ if the i-th position is either the u or v state variables, and $P_i = \sqrt{c_p/T_{\rm r}}$ if the i-th position is the T state variable, otherwise the values are zeros.
- The norm of forecast error variances is the sum of the diagonal elements of

$$\frac{1}{K}\wp\boldsymbol{X}_e(t_{\rm v})\boldsymbol{C}(\boldsymbol{\beta})\boldsymbol{C}^{\rm T}(\boldsymbol{\beta})\boldsymbol{X}_{\rm e}(t_{\rm v})^{\rm T}\wp\,.$$

- The measurement of the adaptive data impact is calculated as follows. Let $\boldsymbol{Z} = (\boldsymbol{Z}, \ldots, \boldsymbol{Z}_M) = \boldsymbol{X}_{\rm e}(t_{\rm v})^{\rm T}\wp$, where $\boldsymbol{Z}_i$ is the i-th column of matrix $\boldsymbol{Z}$. The forecast error J is

$$J[\boldsymbol{\beta}] = \frac{1}{K}\sum_{i=1}^{M}\boldsymbol{Z}_i^{\rm T}\boldsymbol{C}[\boldsymbol{\beta}]\boldsymbol{C}^{\rm T}[\boldsymbol{\beta}]\boldsymbol{Z}_i\,. \tag{9}$$

In general, the forecast error variance reduction in ET at a possible adaptive deployment at a location l is

$$S_l = J[\beta_l = 1] - J[1 - \Delta\beta_l]\,. \tag{10}$$

The forecast error reduction estimations are obtained by repeating the above process for all possible adaptive deployments. In BT1999, it was assumed the analysis error variance is reduced by 0.5 ($\Delta\beta_l = 0.5$).

3. ETS method

By perturbing all possible adaptive observation data, the ET method may yield high order information about the sensitivity regions but it could be costly for high-resolution applications with large ensemble members. In this section, we consider a first order approximation of the ET method, ET sensitivity.

3.1. *ET based sensitivity*

The basic idea of the ETS in this paper is to use the sensitivity (gradient) of forecast error variance over the verification region in terms of analysis error variance to determine data sensitive regions for adaptive observations. It is the first order approximation of Eq. (10), but only a single transformation matrix computation will be needed, thus improving computation efficiency when compared to ET. The main objective is to derive a mathematical formulation of $\partial J/\partial\beta_l$ in this paper.

Following Eq. (8), the gradient of J to the analysis error variance reduction ratio $\boldsymbol{\beta}$ is

$$\begin{aligned}\nabla J &= \left(\frac{\partial J}{\partial\beta_1},\ldots,\frac{\partial J}{\partial\beta_l},\ldots,\frac{\partial J}{\partial\beta_M}\right)^{\mathrm{T}} \\ &= \left(\frac{1}{K}\sum_{i=1}^{M}\boldsymbol{Z}_i^{\mathrm{T}}\frac{\partial\boldsymbol{C}\boldsymbol{C}^{\mathrm{T}}}{\partial\beta_1}\boldsymbol{Z}_i,\ldots,\frac{1}{K}\sum_{i=1}^{M}\boldsymbol{Z}_i^{\mathrm{T}}\frac{\partial\boldsymbol{C}\boldsymbol{C}^{\mathrm{T}}}{\partial\beta_l}\boldsymbol{Z}_i,\ldots,\right. \\ &\quad \left.\frac{1}{K}\sum_{i=1}^{M}\boldsymbol{Z}_i^{\mathrm{T}}\frac{\partial\boldsymbol{C}\boldsymbol{C}^{\mathrm{T}}}{\partial\beta_M}\boldsymbol{Z}_i\right)^{\mathrm{T}} . \qquad (11a)\end{aligned}$$

The estimated forecast error variance reduction is

$$\begin{aligned}dJ &= \left(\frac{1}{K}\sum_{i=1}^{M}\boldsymbol{Z}_i^{\mathrm{T}}\frac{\partial\boldsymbol{C}\boldsymbol{C}^{\mathrm{T}}}{\partial\beta_1}\boldsymbol{Z}_i,\ldots,\frac{1}{K}\sum_{i=1}^{M}\boldsymbol{Z}_i^{\mathrm{T}}\frac{\partial\boldsymbol{C}\boldsymbol{C}^{\mathrm{T}}}{\partial\beta_l}\boldsymbol{Z}_i,\ldots,\right. \\ &\quad \left.\frac{1}{K}\sum_{i=1}^{M}\boldsymbol{Z}_i^{\mathrm{T}}\frac{\partial\boldsymbol{C}\boldsymbol{C}^{\mathrm{T}}}{\partial\beta_M}\boldsymbol{Z}_i\right)^{\mathrm{T}} d\boldsymbol{\beta} . \qquad (11b)\end{aligned}$$

In the BT1999 implementation, $d\boldsymbol{\beta}$ is set to a constant with a value of 0.5. The ET method is approximated by ETS derivatives. In operational applications, $\Delta\boldsymbol{\beta}$ can be set to different values at different locations that can really take advantage of an analysis error covariance, e.g., a large reduction ($\Delta\boldsymbol{\beta}$) occurs over a large analysis error variance.

3.2. *Derivatives of the transformation matrix C formulation*

The main contribution of the ETS method is the derivation of an analytic gradient formulation of $\partial\boldsymbol{C}\boldsymbol{C}^{\mathrm{T}}/\partial\boldsymbol{\beta}$ in Eq. (11a) in terms of the error reduction coefficient β_l.

For the ET transformation matrix $\boldsymbol{C}$, let us introduce a matrix

$$\boldsymbol{\Psi} = K(\boldsymbol{C}\boldsymbol{C}^{\mathrm{T}})^{-1} = \boldsymbol{X}_{\mathrm{e}}(t_{\mathrm{fa}})^{\mathrm{T}}\boldsymbol{A}_{\mathrm{g}}^{-1}\boldsymbol{X}_{\mathrm{e}}(t_{\mathrm{fa}}) . \qquad (12)$$

and then the product of ET transformation matrix $\boldsymbol{C}\boldsymbol{C}^{\mathrm{T}} = K\boldsymbol{\Psi}^{-1}$ as given in Eq. (6). Using an inverse matrix derivative formulation, the ET transformation product derivative is,

$$\frac{\partial\boldsymbol{C}\boldsymbol{C}^{\mathrm{T}}}{\partial\beta_l} = -K\boldsymbol{\Psi}^{-1}\frac{\partial\boldsymbol{\Psi}}{\partial\beta_l}\boldsymbol{\Psi}^{-1} , \qquad (13)$$

where,

$$\begin{aligned}\frac{\partial\boldsymbol{\Psi}}{\partial\beta_l} &= \boldsymbol{X}_{\mathrm{e}}(t_{\mathrm{fa}})^{\mathrm{T}}\frac{\partial\boldsymbol{A}_{\mathrm{g}}^{-1}}{\partial\beta_l}\boldsymbol{X}_{\mathrm{e}}(t_{\mathrm{fa}}) \\ &= -\boldsymbol{X}_{\mathrm{e}}(t_{\mathrm{fa}})^{\mathrm{T}}\boldsymbol{A}_{\mathrm{g}}^{-1}\frac{\partial\boldsymbol{A}_{\mathrm{g}}}{\partial\beta_l}\boldsymbol{A}_{\mathrm{g}}^{-1}\boldsymbol{X}_{\mathrm{e}}(t_{\mathrm{fa}}) . \qquad (14)\end{aligned}$$

Thus, ET sensitivity can be obtained using Eqs. (11–14).

$$\frac{\partial J}{\partial\beta_l} = \sum_{i=1}^{M}\boldsymbol{Z}_i^{\mathrm{T}}\boldsymbol{\Psi}^{-1}\boldsymbol{X}_{\mathrm{e}}(t_{\mathrm{fa}})^{\mathrm{T}}\boldsymbol{A}_{\mathrm{g}}^{-1}\frac{\partial\boldsymbol{A}_{\mathrm{g}}}{\partial\beta_l}\boldsymbol{A}_{\mathrm{g}}^{-1}\boldsymbol{X}_{\mathrm{e}}(t_{\mathrm{fa}})\boldsymbol{\Psi}^{-1}\boldsymbol{Z}_i. \qquad (15)$$

Note the $\partial\boldsymbol{A}_{\mathrm{g}}/\partial\beta_l$ is usually a constant matrix. For an example of a diagonal matrix of $\boldsymbol{A}_{\mathrm{g}} = \mathrm{diag}(\alpha_1\beta_1,\ldots,\alpha_M\beta_M)$ (BT1999), $\partial\boldsymbol{A}_{\mathrm{g}}/\partial\beta_l|_{\beta=1}$ is equal to a diagonal matrix of $\mathrm{diag}(0,\ldots,0,\alpha_l,0,\ldots,0)$. For a given guessed analysis error variance $\boldsymbol{A}_{\mathrm{g}}$, the ET transformation matrix $\boldsymbol{C}\boldsymbol{C}^{\mathrm{T}}$ is determined. So the ET sensitivity from Eq. (15) can be obtained after a single computation of a transformation matrix instead of calculating ensemble transformations ($\boldsymbol{C}[\boldsymbol{\beta}]\boldsymbol{C}^{\mathrm{T}}[\boldsymbol{\beta}]$) for all possible perturbations in ET using Eq. (10).

3.3. *Practical procedure and computation cost*

When applying ETS in practice, Eq. (15) is not solved directly. Here are the implementation procedures:

Step 1: Compute the perturbation fields at the t_{fa} : $\boldsymbol{X}_{\mathrm{e}}(t_{\mathrm{fa}})$, and t_{v} : $\boldsymbol{X}_{\mathrm{e}}(t_{\mathrm{v}})$.

Step 2: Initial the projection matrix $\wp$ and the guessed analysis error variance $\boldsymbol{A}_{\mathrm{g}}$.

Step 3: Compute the inverse of Eq. (12): $\boldsymbol{X}_{\mathrm{e}}(t_{\mathrm{fa}})^{\mathrm{T}}\boldsymbol{A}_{\mathrm{g}}^{-1}\boldsymbol{X}_{\mathrm{e}}(t_{\mathrm{fa}})$

Step 4: Compute the matrix $\boldsymbol{Z}$: $\boldsymbol{Z} = \boldsymbol{X}_{\mathrm{e}}(t_{\mathrm{v}})^{\mathrm{T}}\wp$

Step 5: Obtain all the signals [Eq. (11a)]: $\partial J/\partial\beta_l, l = 1\ldots M$. Decomposition of the $K\times K$ symmetric matrix ($\boldsymbol{C}\boldsymbol{C}^{\mathrm{T}}$) takes $K^3/6$ computing operations (Step 3 costs $\sim K^3/6$). In order to obtain all of the sensitivity, ETS needs to estimate the sensitivity at all the elements in the state vector (M), with an Eq. (11a) cost of $\sim M^2$ (Step 5 costs $\sim M^2$). So, the computation count of ETS is about $M^2+K^3/6$. However, ET needs to decompose the $\boldsymbol{C}\boldsymbol{C}^{\mathrm{T}}$ matrix at each element in the state vector [Eqs. (9) and (10) with a cost of $\sim M^2+K^3/6$] to obtain all

Table 2. Estimated computation counts of ET and ETS.

	$M=10^3$		$M=10^5$		$M=10^7$	
	$K=50$	$K=100$	$K=50$	$K=100$	$K=50$	$K=100$
ETS	1×10^6	1.1×10^6	1×10^{10}	1×10^{10}	1×10^{14}	1×10^{14}
ET	2.08×10^{10}	1.67×10^{11}	2.08×10^{14}	1.67×10^{15}	2.08×10^{18}	1.67×10^{19}

the signals (forecast error reduction). The magnitude of K is about 10^2. The M is 10^3 in a very coarse resolution. It could rise to 10^8 in the high-resolution case. Table 2 shows the estimation of the computation counts of ET and ETS. ETS gains greatly in efficiency as it only needs to decompose the $\boldsymbol{CC}^{\mathrm{T}}$ once. When M and K are large, the difference is significant.

4. Numerical experiments

In this section, we apply ET and ETS for a hurricane case and a rainfall case. The first case, Hurricane Irene (2011), formed on 21 August, and became a hurricane on 22 August 2011. It then passed Exuma and Cat Islands. It made landfall near Cape Lookout, North Carolina at 1200 UTC on 27 August. It continued tracking north northeastward, and moved over Manhattan, New York on 28 August. The heavy rainfall and strong wind caused severe damage (Avila and Stewart, 2012). We also apply ET and ETS for a heavy rainfall case. The heavy precipitation in this case is associated with a low level vortex that developed over western China during 3-5 August 2013. The hourly accumulate precipitation was $>$30 mm over the Beijing areas at 1200 UTC 4 August 2013.

4.1. *Data and experiment setup*

The European Centre for Medium-range Weather Forecasts ensemble forecasts are used in this study, which can be downloaded from the THORPEX Interactive Grand Global Ensemble (TIGGE) portal (http://apps.ecmwf.int/datasets/data/tigge/). The initial time of the ensemble forecasts are at 0000 UTC 24 August 2011 and 1200 UTC 3 August 2013 for the hurricane and heavy rainfall case, respectively. The length of prediction time is 72-h with a 6-h interval for the ensemble prediction outputs. The variables selected for the ET dry energy norm are the temperature and horizontal wind components at the 850, 500 and 200 hPa pressure levels. The diagonal values of guessed analysis error covariance $\boldsymbol{A}_{\mathrm{g}}$ used are the same as ETKF (Majumdar et al., 2002): the guessed analysis error covariance of wind at the 850, 500 and 200 hPa pressure levels is 2.72, 3.16 and 4.66 m s^{-1} separately; the guessed analysis error covariance of temperature at the 850, 500 and 200 hPa pressure levels is 1.22, 0.92°C and 1.82°C separately.

For the hurricane case, the verification area (26°–40°N, 86°–70°W) is marked by the inner rectangle showed in Fig. 1a). The estimation or potential targeting observation area is the whole domain (10°–50°N, 100°–60°W). The ensemble mean indicated that the hurricane was moving towards the east coast of the U.S. at 0000 UTC 27 August, and it is selected as the t_{v} in this case. There are seven t_{fa} for the adaptive observations, -0 h, -12 h, -24 h, -36 h, -48 h, -60 h, and -72 h. The negative hours t_{fa} indicate the number of hours ahead of the t_{v}, correspondingly. For the heavy rainfall case, the verification area is over the Beijing area (38°–42°N, 114°–120°E), (Fig. 1b). The estimation potential targeting area was covered from 100°E to 124°E and 34°N to 50°N. The t_{v} is the heavy rainfall time, 1200 UTC 4 August 2013. The t_{fa} are set to 6 h and 12 h ahead of the t_{v}. As claimed in section 3, ETS is more efficient when the number of ensemble members (K) and the elements in state vectors ($\boldsymbol{M}$) are mathematically large. We set up six experiments (Table 3) with

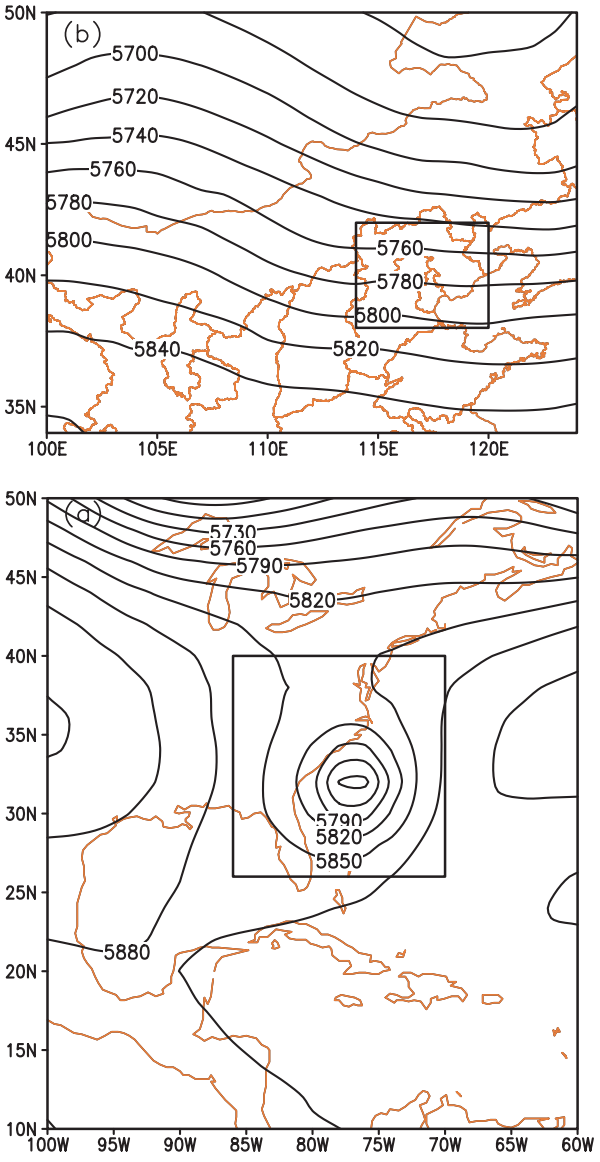

Fig. 1. The domain and verification areas for the (a) Hurricane Irene (2011) and (b) Beijing rainfall cases. Contours are the ensemble mean geopotential height at 500 hPa (gpm). The inner rectangle is the verification areas.

Table 3. Setup of numerical Experiments.

Experiment name	Horizontal resolution	Number of ensemble members
K10R2	$2^\circ \times 2^\circ$	10
K10R1	$1^\circ \times 1^\circ$	10
K30R2	$2^\circ \times 2^\circ$	30
K30R1	$1^\circ \times 1^\circ$	30
K50R2	$2^\circ \times 2^\circ$	50
K50R1	$1^\circ \times 1^\circ$	50

different resolutions and ensemble members to demonstrate this claim numerically. The number of ensemble members vary from 10 to 30 to 50. Two resolutions are used, $1^\circ \times 1^\circ$ and $2^\circ \times 2^\circ$. As an example, K30R1 means the number of ensemble members is 30 and the resolution is $1^\circ \times 1^\circ$.

4.2. *Summary map*

A summary map—the signals of sensitivity identified by ET or ETS over the whole calculation domain—shows the sensitive area. ET considered each grid point as a hypothetical adaptive site and identified sensitive areas by perturb-

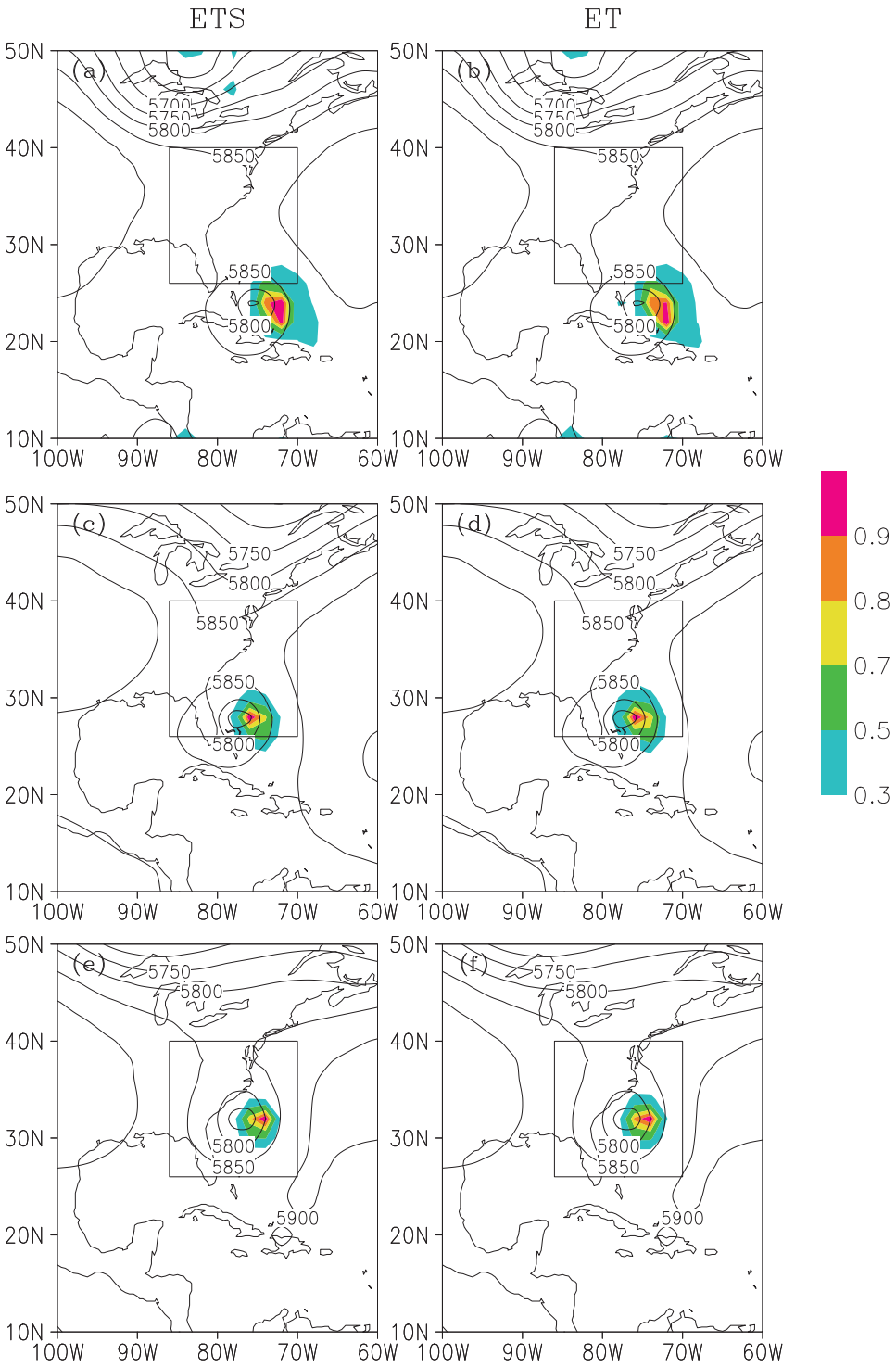

Fig. 2. The signals (color filled areas) identified by (a, c, e) ETS and (b, d, f) ET at a different t_a in K30R2 for the Hurricane Irene case. The t_a are (a, b) 0000 UTC 25 August; (c, d) 0000 UTC 26 August, (e, f) 0000 UTC 27 August. The contours are the 500 hPa geopotential height of the ensemble mean forecast at each t_a. The inner rectangle is the verification area. The t_v is 0000 UTC 27 August.

ing the analysis error variance at each observation site. The signal—the reduction of forecast error covariance associated with this grid point—can be obtained. The summary map can be plotted after perturbing the variance and calculating the reduction over all the grid points.

In contrast to these perturbations of ET, the ETS method can obtain these values by a single computation of the derivative, using the same amount of computation as would be needed for each individual ET perturbation. The derivatives are shown, as well as the reduction of analysis error variance. They represent the sensitivity signals over the calculation domain.

In order to compare the signals from ETS and ET at different t_{fa}, the signals from Eqs. (10) and (15, 11b) are normalized in this study,

$$\overline{\boldsymbol{S}} = (\boldsymbol{S} - S_{\min})/(S_{\max} - S_{\min}) \,, \tag{16}$$

where $S_{\max}/S_{\min}$ are the maximum/minimum values over the whole domain. Thus, the summary maps show the relative sensitivity of the ET or ETS methods.

4.3. *Sensitive areas identified by ET and ETS*

The color filled areas of Fig. 2 show the normalized signals identified by ET and ETS at different t_{fa} for experiment K30R2 in the hurricane case. It is seen that ETS and ET give similar signal patterns and evaluation. As the t_{fa} approached the t_v, the signal (color filled contour areas) approached the verification areas. The sensitivity areas are distributed around the hurricane itself, and evolved into the verification areas at the t_v. Figure 3 shows the normalized signals identified from ET and ETS from K50R2 and K10R1. The results are very close to K30R2. The signals are both located at the hurricane's eastern center. It shows that the data sensitive region identified by ETS is very close to ET even when the results

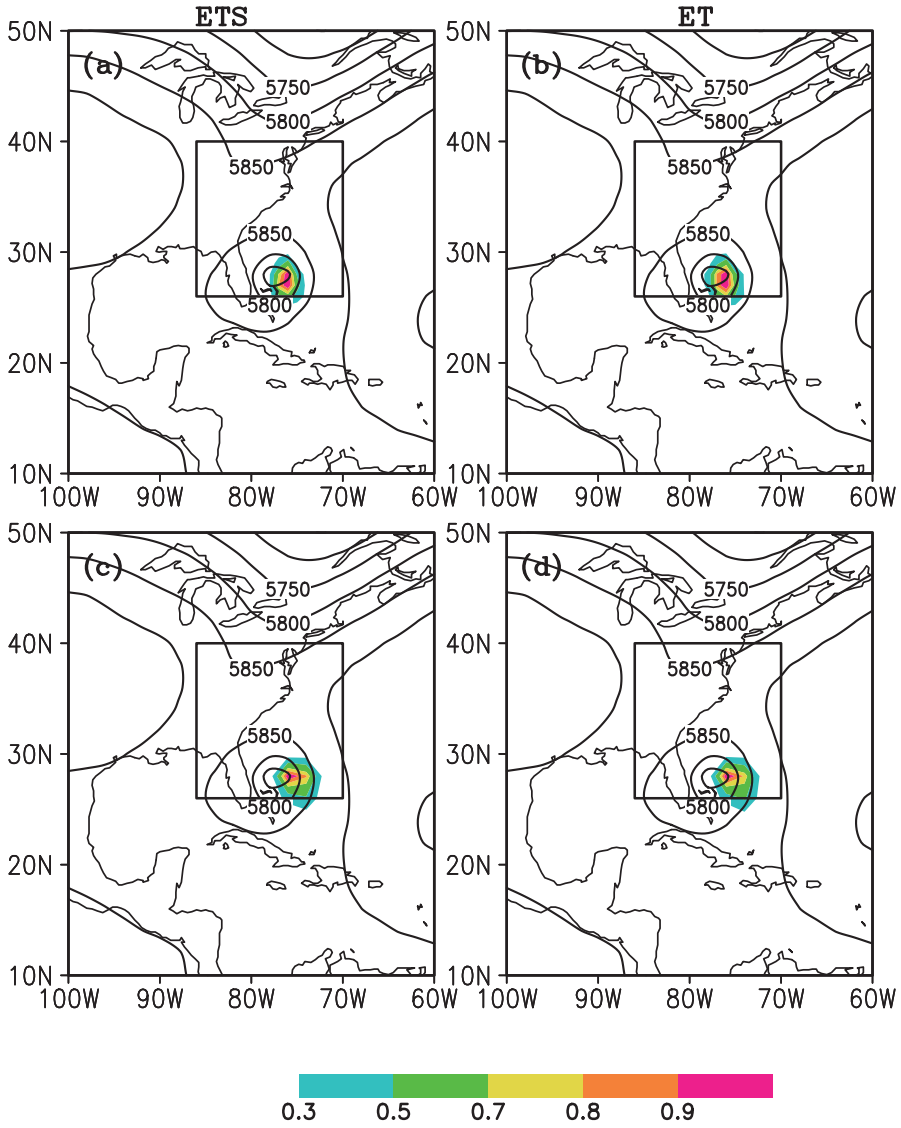

Fig. 3. The signals (color-filled areas) identified by (a, c) ETS and (b, d) ET in the Hurricane Irene case: (a, b) are Experiment K50R1; (c, d) experiment K10R2. The t_a is 0000 UTC 26 August 2011. The contours are the 500 hPa geopotential height of ensemble mean forecasts.

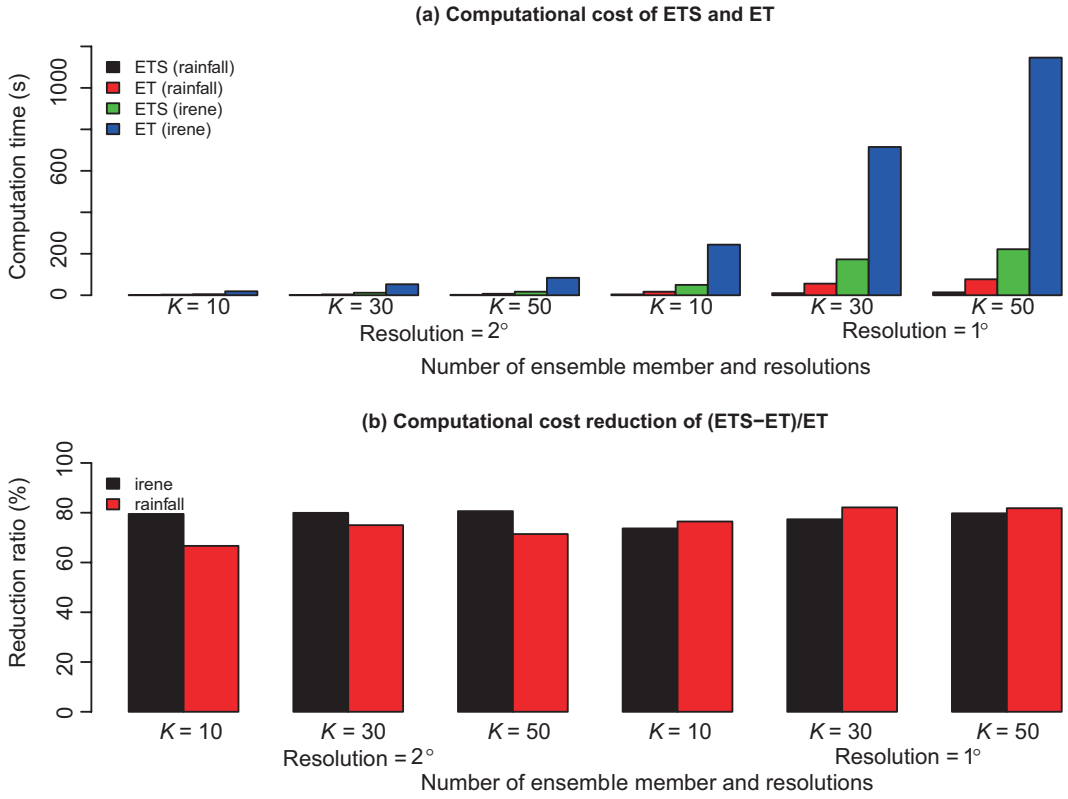

Fig. 4. (a) Computational cost of different experiments. (b) Relative computation time reduction.

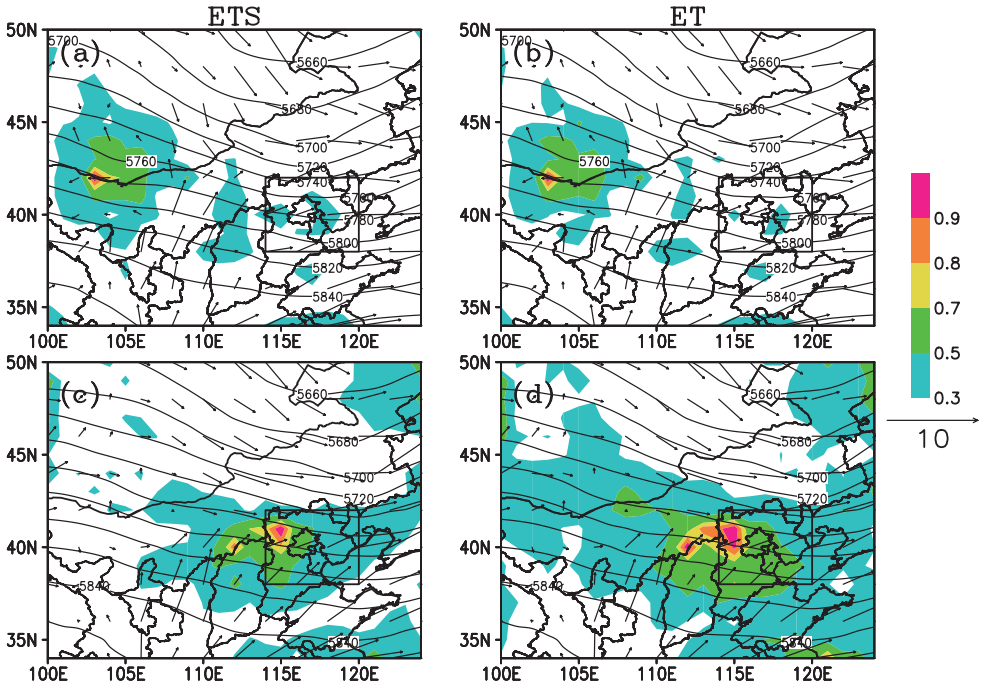

Fig. 5. The signals (color filled areas) identified by (a, c) ETS and (b, d) ET in K30R2 for the Beijing rainfall case. The t_v is 1200 UTC 4 August 2013. The t_a are (a, b) is 0000 UTC 4 August; (c, d) 0600 UTC 4 August. The wind barbs are the horizontal wind component at 850 hPa (units: m s^{-1}). The contours are the 500 hPa geopotential height of the ensemble mean forecast at each t_a. The inner rectangle is the verification area.

are from a different number of ensemble members and resolutions. Generally, the ETS can obtain the same sensitive areas as ET without high consumption.

ETS is much faster than ET because ET needs to loop over all the possible elements in the state vector (M), especially when the number of ensemble prediction members (K) is large. Figure 4 shows the computational costs and relative computation time reduction with ETS and ET using a different number of ensemble prediction members (K). The cost is less than 60 seconds with a fine resolution and few ensemble prediction members for ETS and ET. This is acceptable for the adaptive observations. However, the computational cost rises to about 1200 seconds with a $1^\circ \times 1^\circ$ resolution in the horizontal direction, with three vertical levels and 50 ensemble prediction members. ETS only costs about 200 seconds. Overall, the computation time saved by ET was 60%–80% (Fig. 4b). If the computational domain is larger (particularly for a global model) with higher resolution in the horizontal and vertical directions (here the computations were conducted in three vertical levels only), the reduction in computational costs would be much more significant with ETS compared to ET.

The signals from the heavy rainfall case are shown in Fig. 5. It can be seen that the signals are similar between ET and ETS. The sensitive areas were distributed around the wind divergence (850 hPa) and the trough (500 hPa) at 12 hours ahead of the t_v (Figs. 5a and b). The signals are located in the west of the verification areas at 6 hours ahead of the t_v (Figs. 5c and d). Although the sensitive areas from the ET covered a slightly larger area compared to ETS, signals with maximum values are located at almost the same position in ET and ETS. The following section provides more discussion on the differences between ETS and ET.

4.4. *Differences between ET and ETS*

In BT1999, the signals are calculated by Eq. (10). ETS used Eq. (15) to calculate the signals. So ETS is a first order approximation of the ET. This also means the results from ETS should get closer to those of ET when $\Delta\boldsymbol{\beta}$ approaches zero. Here we set up three more numerical experiments using different $\Delta\boldsymbol{\beta}$ values for ET ($\Delta\boldsymbol{\beta} = 0.2, 0.4, 0.6$). When $\Delta\boldsymbol{\beta} = 0.2$ this means the ET signals are estimated by: $s_l = J[\beta_l = 1] - J[\beta_l = 0.8]$ It is noted that ETS signals [Eqs. (10a), (14)] do not vary with different $\Delta\boldsymbol{\beta}$. Figures 6 and 7 show the ETS and ET signals for the Hurricane Irene (2011) and Beijing rainfall cases, respectively. The differences be-

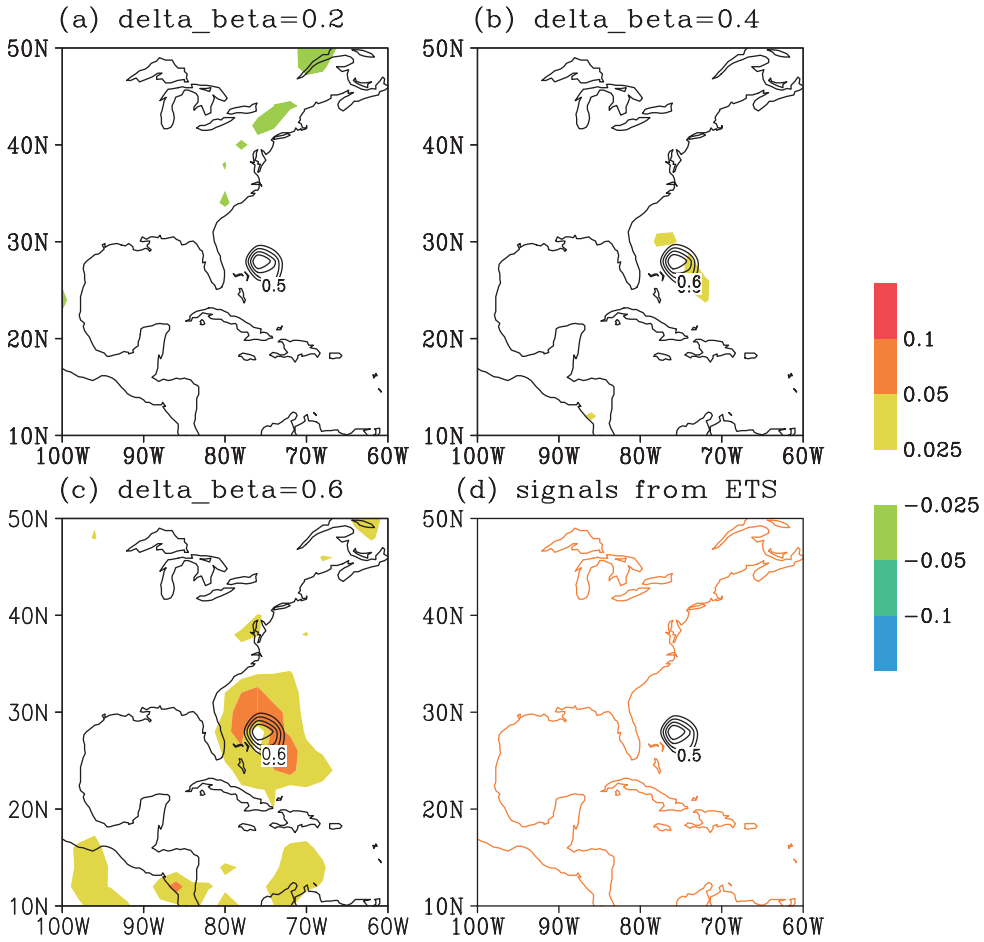

Fig. 6. The signals for the Hurricane Irene (2011) case. Contours are the signals from (a–c) ET and (d) ETS. The experiment is K30R2. The t_a is 0000 UTC 26 August 2011. Color filled areas show the signal differences between ETS and ET. The analysis error reduction for ET is (a) 0.2, (b), 0.4 and (c) 0.6.

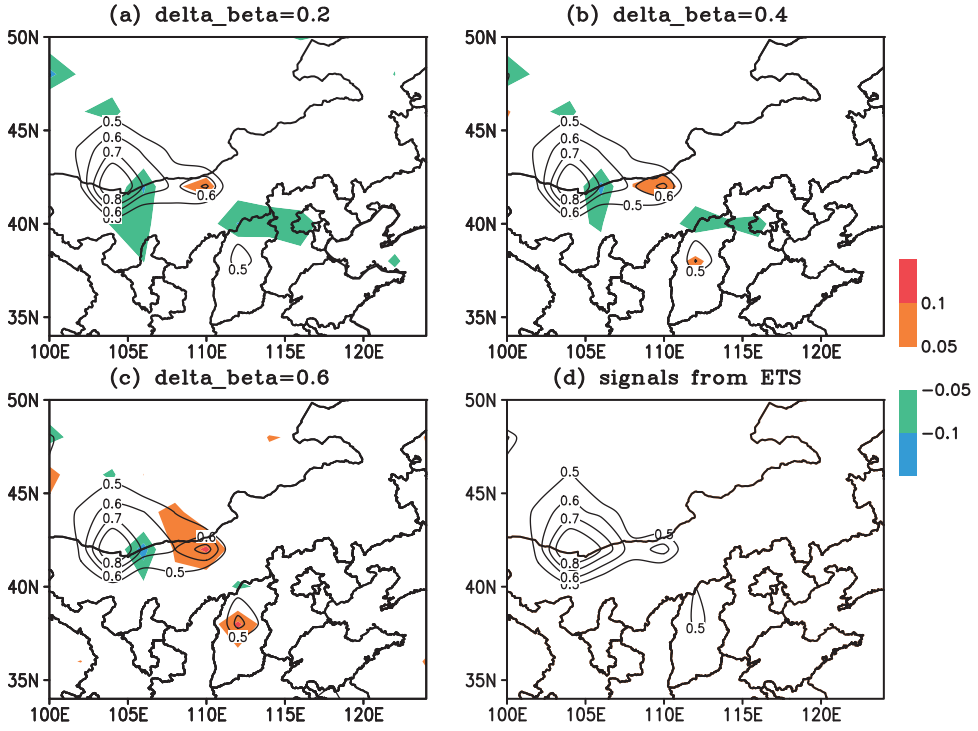

Fig. 7. As in Fig. 6 but for the rainfall case. The t_a is 0000 UTC 4 August 2013.

tween ETS and ET are presented by the color shading colors. It is seen that for the smallest $\Delta\boldsymbol{\beta}$, the two methods produce almost the same data sensitive region (Figs. 6 and 7). And for larger values of $\Delta\boldsymbol{\beta}$, the ETS signal distribution is still close to the ET signal; in particular, the centers of the signals from the two methods are almost the same even with a large $\Delta\boldsymbol{\beta}$. Overall, for the Hurricane Irene (2011) case, both ET and ETS identify one sensitive region (Fig. 6); for the rainfall case, one region with global maximum signals and two local regions with local maximum signals (Fig. 7) are identified. The differences between ET and ETS are acceptable, since the targeting observation focuses on the sensitive areas with a maximum (the center of the signals). Generally the signals from ET and ETS are similar.

5. Conclusion and discussion

Adaptive observations have the potential to improve weather forecasts. Among existing methods of identifying observation sensitivity regions, ET is attractive because of its use of analysis error covariance information and its efficiency compared to other more complex methods. In this study, a newly proposed ETS approach for adaptive observations is derived and demonstrated. The ETS method only uses a single computation of a transformation matrix to yield a sensitivity summary map, instead of calculating ensemble transformations for all possible perturbations, as in the ET method. Thus, it further increase the computational efficiency. If the computational domain is larger (even global in the horizontal direction), with higher resolution in the horizontal and vertical directions, the reduction in computational cost would be far greater with ETS compared to ET. Numerical experiments with Hurricane Irene (2011) and a heavy rainfall case in Beijing showed that ETS reduced the computation cost by 60%–80%.

The summary maps from the two cases show that the ETS method produces a similar data sensitive region as the ET method, especially for the region with large signal values. Thus, the new method gains computational efficiency without losing the positive characteristics of the ET method. It is noted that, in general, the more realistic the analysis covariance is, the better the targeting region is that can be identified under the assumption of ET. As the main aim of this paper is mainly to introduce the ETS method, the best guess of analysis covariance, which can be provided by a data assimilation system (e.g., ETKF), will be further studied in future work. Our plan is to implement ETS at the NCEP Environmental Modeling Center for WSR, and compare it to the existing ET adaptive observation method in future works. With its improved efficiency, ETS can be applied to severe weather events with high spatial resolution and a large number of ensemble members.

Acknowledgements. The authors thank John C. OSBORN at NOAA Earth System Research Laboratory for his English editorial support on this manuscript. The authors would like to express their appreciation to the two anonymous reviewers for their comments on the earlier version of the manuscript, which helped improve the presentation of this paper. This work was jointly sponsored by the Key Project of the Chinese National Programs for Fundamental Research and Development (“973 Program”, Grant No. 2013CB430106), and

the Key Project of the Chinese National Science & Technology Pillar Program during the Twelfth Five-year Plan Period (Grant No. 2012BAC22B01).

REFERENCES

Aberson, S. D., 2003: Targeted observations to improve operational tropical cyclone track forecast guidance. *Mon. Wea. Rev.*, **131**, 1613–1628.

Aberson, S. D., S. J. Majumdar, C. A. Reynolds, and B. J. Etherton, 2011: An observing system experiment for tropical cyclone targeting techniques using the global forecast system. *Mon. Wea. Rev.*, **139**, 895–907.

Ancell, B., and G. J. Hakim, 2007: Comparing adjoint- and ensemble-sensitivity analysis with applications to observation targeting. *Mon. Wea. Rev.*, **135**, 4117–4134.

Anderson, J. L., 1997: The impact of dynamical constraints on the selection of initial conditions for ensemble predictions: Low order perfect model results. *Mon. Wea. Rev.*, **125**, 2969–2983.

Avila, L. A., and S. Stewart, 2012: Atlantic hurricanes 2011: All about Irene and Lee. *Weatherwise*, **65**, 34–41.

Bauer, P., R. Buizza, C. Cardinali, and J.-N. Thépaut, 2011: Impact of singular vector based satellite data thinning on NWP. *Quart. J. Roy. Meteor. Soc*., **137**, 286–302.

Berger, H., R. Langland, C. S. Velden, C. A. Reynolds, and P. M. Pauley, 2011: Impact of enhanced satellite-derived atmospheric motion vector observations on numerical tropical cyclone track forecasts in the western North Pacific during TPARC/TCS-08. *J. Appl. Meteor. Climatol*., **50**, 2309–2318.

Bishop, C. H., and Z. Toth, 1999: Ensemble transformation and adaptive observations. *J. Atmos. Sci.*, **56**, 1748–1765.

Bishop, C. H., B. J. Etherton, and S. J. Majumdar, 2001: Adaptive sampling with the ensemble transform Kalman filter. Part I: Theoretical aspects. *Mon. Wea. Rev.*, **129**, 420–436.

Buizza, R., and A. Montani, 1999: Targeted observations using singular vectors. *J. Atmos. Sci.*, **56**, 2965–2985.

Chang, E. K. M., M. H. Zheng, and K. Raeder, 2013: Medium-range ensemble sensitivity analysis of two extreme pacific extratropical cyclones. *Mon. Wea. Rev.*, **141**, 211–231.

Chou, K.-H., C.-C. Wu, P.-H. Lin, S. D. Aberson, M. Weissmann, F. Harnisch, and T. Nakazawa, 2011: The impact of dropwindsonde observations on typhoon track forecasts in DOTSTAR and T-PARC. *Mon. Wea. Rev*., **139**, 1728–1743.

Ehrendorfer, M., R. M. Errico, and K. D. Raeder, 1999: Singular-vector perturbation growth in a primitive equation model with moist physics. *J. Atmos. Sci*., **56**, 1627–1648.

Hamill, T. M., J. S. Whitaker, and C. Snyder, 2001: Distance-dependent filtering of background error covariance estimates in an ensemble Kalman filter. *Mon. Wea. Rev.*, **129**, 2776–2790.

Ito, K., and C.-C. Wu, 2013: Typhoon-position-oriented sensitivity analysis. Part I: Theory and verification. *J. Atmos. Sci.*, **70**, 2525–2546.

Joly, A., and Coauthors, 1997: The fronts and Atlantic storm-track experiment (FASTEX): Scientific objectives and experimental design. *Bull. Amer. Meteor. Soc.*, **78**, 1917–1940.

Joly, A., and Coauthors, 1999: Overview of the field phase of the fronts and Atlantic Storm-Track EXperiment (FASTEX) project. *Quart. J. Roy. Meteor. Soc.*, **125**, 3131–3163.

Langland, R. H., R. Gelaro, G. D. Rohaly, and M. A. Shapiro, 1999a: Targeted observations in FASTEX: Adjoint-based targeting procedures and data impact experiments in IOP17 and IOP18. *Quart. J. Roy. Meteor. Soc.*, **125**, 3241–3270.

Langland, R. H., and Coauthors, 1999b: The North Pacific experiment (NORPEX-98): Targeted observations for improved North American weather forecasts. *Bull. Amer. Meteor. Soc.*, **80**, 1363–1384.

Majumdar, S. J., C. H. Bishop, B. J. Etherton, I. Szunyogh, and Z. Toth, 2001: Can an ensemble transform Kalman filter predict the reduction in forecast-error variance produced by targeted observations? *Quart. J. Roy. Meteor. Soc*., **127**, 2803–2820.

Majumdar, S. J., C. H. Bishop, B. J. Etherton, and Z. Toth, 2002: Adaptive sampling with the ensemble transform Kalman filter. Part II: Field program implementation. *Mon. Wea. Rev.*, **130**, 1356–1369.

Majumdar, S. J., and Coauthors, 2011: Targeted observations for improving numerical weather prediction: An overview. WWRP/THORPEX No. 15.

Mu, M., F. F. Zhou, and H. L. Wang, 2009: A method for identifying the sensitive areas in targeted observations for tropical cyclone prediction: Conditional nonlinear optimal perturbation. *Mon. Wea. Rev.*, **137**, 1623–1639.

Palmer, T. N., R. Gelaro, J. Barkmeijer, and R. Buizza, 1998: Singular vectors, metrics, and adaptive observations. *J. Atmos. Sci.*, **55**, 633–653.

Szunyogh, I., Z. Toth, R. E. Morss, S. J. Majumdar, and C. H. Bishop, 2000: The effect of targeted dropsonde observations during the 1999 winter storm reconnaissance program. *Mon. Wea. Rev.*, **128**, 3520–3537.

Szunyogh, I., Z. Toth, A. V. Zimin, S. J. Majumdar, and A. Persson, 2002: Propagation of the effect of targeted observations: The 2000 winter storm reconnaissance program. *Mon. Wea. Rev*., **130**, 1144–1165.

Wang, H. L., M. Mu, X. Y. Huang, 2011: Application of conditional non-linear optimal perturbations to tropical cyclone adaptive observation using the weather research forecasting (WRF) model. *Tellus A*, **63**, 939–957.

Wu, C.-C., K.-H. Chou, P.-H. Lin, S. D. Aberson, M. S. Peng, and T. Nakazawa, 2007a: The impact of dropwindsonde data on typhoon track forecasts in DOTSTAR. *Wea. Forecasting*, **22**, 1157–1176.

Wu, C.-C., J.-H. Chen, P.-H. Lin, and K.-H. Chou, 2007b: Targeted observations of tropical cyclone movement based on the adjoint-derived sensitivity steering vector. *J. Atmos. Sci.*, **64**, 2611–2626.

Wu, C.-C., S.-G. Chen, J.-H. Chen, K.-H. Chou, and P.-H. Lin, 2009: Interaction of Typhoon Shanshan (2006) with the mid-latitude trough from both adjoint-derived sensitivity steering vector and potential vorticity perspectives. *Mon. Wea. Rev.*, **137**, 852–862.

Xie, B. G., F. Q. Zhang, Q. H. Zhang, J. Poterjoy, and Y. H. Weng, 2013: Observing strategy and observation targeting for tropical cyclones using ensemble-based sensitivity analysis and data assimilation. *Mon. Wea. Rev.*, **141**, 1437–1453.